2-17-2020

Robustness of Optical Response for Self-Assembled Plasmonic Metamaterials with Morphological Disorder and Surface Roughness

Nian-Hai Shen
Iowa State University and Ames Laboratory

Md Mir Hossen
Iowa State University and Ames Laboratory

Andrew C. Hillier
Iowa State University and Ames Laboratory, hillier@iastate.edu

Thomas Koschny
Iowa State University and Ames Laboratory, koschny@ameslab.gov

Costas M. Soukoulis
Iowa State University, Ames Laboratory, and Foundation for Research and Technology Hellas, soukouli@ameslab.gov

Robustness of Optical Response for Self-Assembled Plasmonic Metamaterials with Morphological Disorder and Surface Roughness

Abstract

Bottom-up fabrication of metallized biotemplated nanostructures to form specific plasmonic nanoresonators holds promise as a means of achieving large-scale optical metamaterials. However, in contrast to top-down methods, the stochastic growth of self-assembled nanoresonators is prone to significant disorder and surface roughness, which naturally raise an important question about the robustness of their resonant properties in terms of structural imperfections. An aggregated-random-sphere model is developed to mimic the nucleated growth of metallized DNA origami assembly, leading to meta-atoms with realistic, experimentally observed morphological disorder and surface roughness. Using the well-known split-ring-resonator (SRR) motif as an example, the resonant properties of meta-atoms under different levels of roughness are investigated and a strong tolerance of optical response against morphological disorder is revealed. It is found that in SRRs, even with dramatic roughness introduced, the expected resonances are still observed, despite broadening line shapes compared to ideal smooth structure. Only for extreme disorder, which causes drastic segmentation of SRRs, does the resonant response disappear. The demonstrations are very encouraging for the prospects of bottom-up fabrication toward versatile functional metamaterials and metadevices.

Keywords

metamaterials, metasurfaces, morphological disorder, surface roughness, self-assembly, DNA origami

Disciplines

Materials Science and Engineering

Robustness of Optical Response for Self-Assembled Plasmonic Metamaterials with Morphological Disorder and Surface Roughness

Nian-Hai Shen,[1,2,*] Md Mir Hossen,[1,3] Andrew C. Hillier,[1,3] Thomas Koschny,[1,2] and Costas M. Soukoulis[1,2,4]

[1]*Division of Materials Science and Engineering, Ames Laboratory—U.S. DOE, Ames, Iowa 50011, USA*

[2]*Department of Physics and Astronomy, Iowa State University, Ames, Iowa 50011, USA*

[3]*Department of Chemical and Biological Engineering, Iowa State University, Ames, Iowa 50011, USA*

[4]*Institute of Electronic Structure and Lasers (IESL), FORTH, 71110 Heraklion, Crete, Greece*

(Dated: December 16, 2019)

This is the author manuscript accepted for publication and has undergone full peer review but has not been through the copyediting, typesetting, pagination and proofreading process, which may lead to differences between this version and the Version of Record. Please cite this article as doi: 10.1002/adom.201901794

Abstract

Bottom-up fabrication of metallized bio-templated nanostructures to form specific plasmonic nano-resonators holds promise as a means of achieving large-scale optical metamaterials. However, in contrast to top-down methods, the stochastic growth of self-assembled nanoresonators is prone to significant disorder and surface roughness, which naturally raise an important question about the robustness of their resonant properties in terms of structural imperfections. We develop an aggregated-random-spheres model to mimic the nucleated growth of metallized DNA origami assembly, leading to meta-atoms with realistic, experimentally observed morphological disorder and surface roughness. Using the well-known split-ring-resonator (SRR) motif as an example, we investigate the resonant properties of meta-atoms under different levels of roughness and reveal a strong tolerance of optical response against morphological disorder. We find that SRRs, even with dramatic roughness introduced, the expected resonances are still observed, despite broadening line-shapes compared to ideal smooth structure. Only for extreme disorder, which causes drastic segmentation of SRRs, does the resonant response disappear. Our demonstrations are very encouraging for the prospects of bottom-up fabrication toward versatile functional metamaterials and metadevices.

Keywords: metamaterials, metasurfaces, morphological disorder, surface roughness, self-assembly, DNA origami

INTRODUCTION

In the past two decades, the concept of metamaterials, i.e., artificial composites based on judiciously designed subwavelength building blocks (meta-atoms), has opened up unprecedented opportunities in tailoring wave propagation for a wealth of new functionalities across many disciplines of science and engineering [1–7]. Significant development in micro- and nano-fabrication methods [8] has greatly advanced the realization of various metadevices, enabling versatile practical applications ranging from the terahertz up to the visible regime [9–15]. To date, most of functional metamaterials and metasurfaces (the two-dimensional form of metamaterials) [16–21] have been fabricated with traditional top-down approaches, such as electron-beam lithography [22], nanoimprinting [23, 24] and direct laser writing [25]. However, due to the complex architectures of meta-atoms, these top-down fabrication methods are generally expensive and time consuming, severely limiting the scalability and feasibility to achieve macroscopic-sized materials and devices. Bottom-up fabrication technologies, such as molecular self-assembly [26] and recently invented DNA origami [27], are promising strategies capable of mitigating these drawbacks and achieving large-scale optical metamaterials. These bio-inspired self-assembled structures can then be harnessed as templates, by transferring their complex spatial information into metal nanostructures, to further build novel plasmonic materials and devices for diverse functionalities [28–32]. Such procedures are challenging yet can be achieved via different approaches, including direct nanoparticle patterning [29, 33], chemical growth of seeded particles [34–39], and DNA-assisted lithography [40]. Nevertheless, the resulting plasmonic structures are prone to possess morphological disorder and surface roughness inherently associated with the stochastic nature of the self-assembly and growth processes.

Metasurfaces are designed to form effective materials where the optical properties are determined by the *averaged* response of the constitutive sub-wavelength nano-resonators (meta-atoms) on a length scale much larger than the unit cell or the average spatial separation between meta-atoms. Therefore, the scattering from a metasurface is expected to exhibit a certain degree of invariance or robustness against disorder in the local microscopic response of the meta-atoms. However, for any practical application the characteristics of the particular type of disorder must be understood and properly modeled; its effect on the optical of the metasurface response must be quantified. Too much disorder will certainly

destroy the resonant response of a metasurface, but how much is too much? There have been various studies of the effect of disorder on the effective resonant response of metamaterials, both theoretical and experimental. Early attempts have studied deviations from perfect spatial periodicity of the same meta-atoms [41], analytic models with randomly distributed parameters of abstract local linear resonant scatterers [42, 43], followed by studies of randomly changing local geometric parameters of physical meta-atoms that constitute three-dimensional metamaterials [44–46]. All find resonance broadening and disorder-induced loss to varying degree. This indicates that for a predictive evaluation of tolerable disorder the actual disorder mechanism and morphology of the metasurface are critical and need to be considered for the specific application.

The examples of our preliminary experimental samples shown in Fig. 1(a) serve to motivate the structure and morphology of our theoretical model of metallized DNA meta-atoms [39], whereby an important question naturally arises about the robustness of the optical response of metamaterials fabricated by this specific approach. In this paper, we will address this problem by applying different levels of morphological disorder and random surface roughness to meta-atoms and statistically analyzing their influence to the optical response of the metamaterial. We will demonstrate surprising levels of tolerance of the fundamental resonant modes of the subwavelength meta-atoms against both experimentally relevant levels of morphological disorder and surface roughness as well as the weak impact of meta-atom density through inter-unit-cell interaction. These results provide strong support for the feasibility of the bottom-up approach of self-assembled DNA-templated metallized nano-resonators for meta-atoms and present important guidance for both theoretical and experimental investigations toward future optical nano-structured materials. Metallized DNA-templated self-assembly of specifically shaped plasmonic nano-resonators as a means to fabricated meta-atoms for optical metasurfaces (and, potentially, bulk metamaterials) is of great real-life interest as it may provide the solution for the scaling problem of optical metamaterials and metasurfaces beyond "purely academic" sized samples. The relevance for the experiment is that our numerical investigation provides (i) quantitative insight into how the specific nature of the experimentally motivated model of morphological disorder inherent to this type of bottom-up self-assembly will effect the optical properties of the desired metasurface and (ii) to provide approximate upper bound on how much morphological disorder and roughness is tolerable in order to still produce an experimentally observable resonant

response of the metasurface fabricated by this method. The latter point is especially important to provide some guidance to the fabrication as to how to optimized the metallization and what levels of seeding density and repeated metallization cycles are required to achieve acceptably smooth surfaces such that the self assembled meta-atoms behave comparably to their lithographically fabricated analogs.

RESULTS AND DISCUSSION

We choose the well-known split-ring-resonator (SRR) motif as an example of a metamaterial building block that is capable of producing a magnetic resonant response at wavelength down to the near infrared [2, 4, 5, 47]. With the magnetic resonance being targeted near the telecommunication wavelength $\lambda \sim 1.55$ μm, a designed SRR unit with ideal shape profile is schematically shown in Figs. 1(b) and (c): the width and thickness of the ring are 40 and 20 nm, respectively, the gap size $g = 10$ nm, and the inner diameter $d = 60$ nm. Thus the outer diameter of the ring is 140 nm, making the size of the meta-atom about an order of magnitude smaller than the wavelength of light at resonance. In our following studies, we consider the SRRs are made of silver (Ag), which is modeled with the measured data of complex permittivity (ϵ) by Johnson and Christy [48], and are excited under normal incidence with the electric field $\boldsymbol{E}$ parallel to the gap to effectively induce the deep-subwavelength magnetic response of interest [see Fig. 1(c)]. For simplicity, we assume the SRRs to be free-standing to focus on the optical responses of SRR itself and set in a periodic array with lattice constant a, forming an SRR metasurface for investigations. Performing numerical scattering simulations using the commercial software COMSOL Multiphysics, we can easily obtain the scattering properties including both reflection (R) and transmission (T) information of the metasurface (for details see the Supporting Information, section VIII). From the scattering amplitudes, we retrieve its effective sheet electric conductivity (σ_e) via the relationship of $\sigma_e = 2(1 - R - T)/(1 + R + T)$, where σ_e has been normalized with respect to the wave impedance ζ and is dimensionless [49]. The retrieved spectrum of σ_e for the ideal SRR with $a = 400$ nm is presented in the upper part of Fig. 1(d) (solid curve is for Re[σ_e] and dashed curve for Im[σ_e]). As expected, we see two resonant features: the magnetic mode occurs at $\sim$185 THz and the electric dipole mode at $\sim$519 THz. Note that the response of the ideal SRR at the side of the electric dipole resonance over 350 THz is scaled by 1/3 of the

original values, in order to clearly show the magnetic resonance (fundamental mode), which is of particular interest. It is convenient to discuss the scattering response of a metasurface in terms of its effective complex electric (and magnetic) sheet-conductivities σ_e (and σ_m) as these quantities uniquely describe the electromagnetic behavior of the metasurface in the effective medium limit. However, we also present the corresponding scattering and absorption cross-sections in section IV of the Supporting Information.

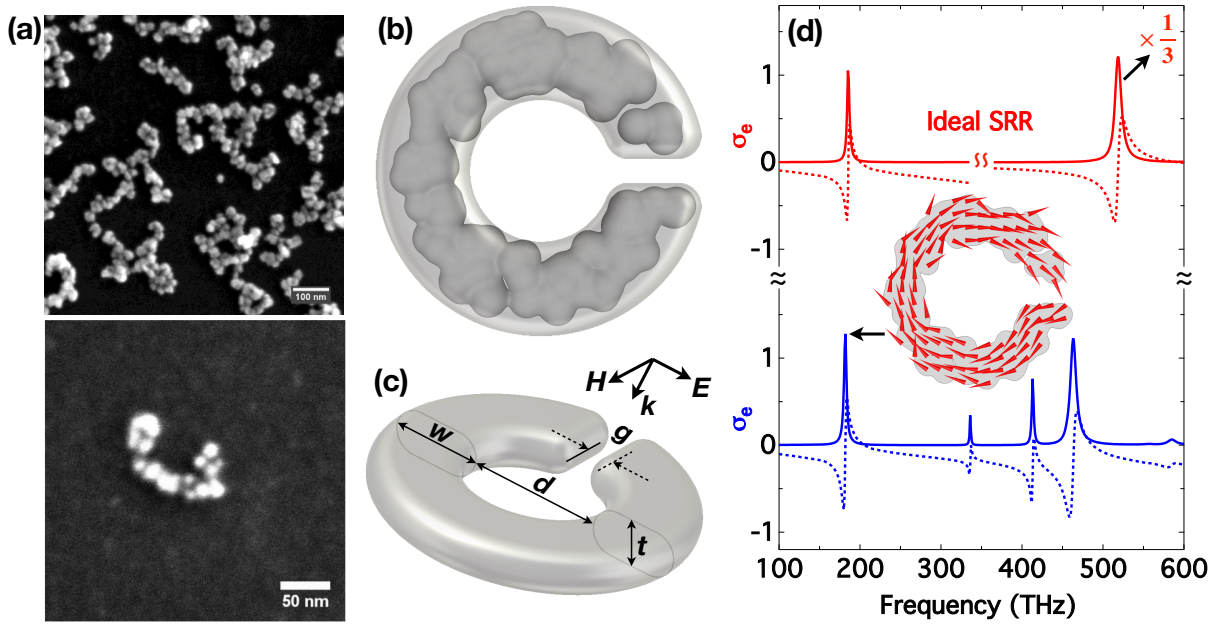

FIG. 1. Simulation of self-assembled metallized DNA origami metamaterial elements via aggregated-random-spheres model to capture effects of morphological disorder and surface roughness. (a) Example SEM images of typical experimentally fabricated metallized-DNA nanoresonators grown by electroless metallization of DNA-origami templates to illustrate realistic morphology and roughness. (b) An example of a "moderately rough" SRR constructed by 120 random spheres, with radius between 8 to 9 nm, accumulating inside of the shape-profile of the ideal SRR. (c) Schematic of the SRR unit under excitation with indicated polarization, where inner diameter d, width w and thickness t of the ring are 60, 40, and 20 nm, respectively, and the gap size $g = 10$ nm. (d) Comparison of retrieved sheet electric conductivity σ_e between the ideal SRR (top) and the example "moderately rough" SRR (bottom). The inset shows the circulating current distribution at 182 THz, corresponding to the electrically-induced magnetic resonance mode.

Referring to the scanning electron microscopy (SEM) images of example metal nanostructures self-assembled from DNA origami as shown in Fig. 1(a), we find it is reasonable to

approximate the random disordered structure of the metallized-DNA building blocks with a disordered aggregation of random solid spheres confined to the volume shape of the SRR as a model to realistically capture both morphological disorder and surface roughness of the meta-atoms (details of this construction are provided in the Supporting Information, section VIII). We firstly introduce a moderate level of surface roughness to the designed SRR by settling inside of the SRR outline 120 spheres at random positions, with radii chosen randomly between 8 to 9 nm, and then generating an ensemble of 100 sample SRRs, which are varied in morphology and even in topology (see the Supporting Information, section I). From the sampling at this level of roughness (denoted as "moderately rough" SRRs hereafter), we arbitrarily picked No. 82 as an example and show it in Fig. 1(b), aligned with the ideal SRR for an intuitive comparison. Following the same procedure of numerical simulation and retrieval, in the bottom part of Fig. 1(d), we show the spectrum of σ_e for this specific "moderately rough" SRR with $a = 400$ nm under the same external excitation. In contrast to the σ_e-spectrum of the ideal SRR, we see multiple resonance features throughout the frequency band of 100-600 THz for the "moderately rough" SRR. However, the circulating current distribution presented in the inset of Fig. 1(d) confirms that the prominent feature at around 182 THz indeed corresponds to our targeted magnetic resonance, with the strength comparable to that of the ideal SRR. In addition, the specific morphology of the structure results in the excitation of some hybridized modes, leaving several extra resonance features above 300 THz in Fig. 1(d). When we survey all the retrieved σ_e spectra of the 100 sample "moderately rough" SRRs (see the Supporting Information, section I), we surprisingly find that the magnetic mode always survives between 100-300 THz regardless of the detailed morphology and topology of the SRR, showing fairly strong robustness of the fundamental resonance of the meta-atom.

In our above discussions, the spacing between SRRs, a, was assumed to be 400 nm. Provided the outer dimension of the SRR itself is $\sim$140 nm as designed, we can consider the in-plane filling ratio or density of SRRs, ρ, to be approximately 7/20. In the view of DNA self-assembled metasurfaces, ρ is in fact a very important factor in determining the overall optical responses of the system. Therefore, here we explore this behavior to identify the level of ρ, at which, the mutual coupling of building blocks can be negligible. The investigations are conducted based on systems of supercells constructed with different SRRs, since this not only allows us to see the collective response of different composing

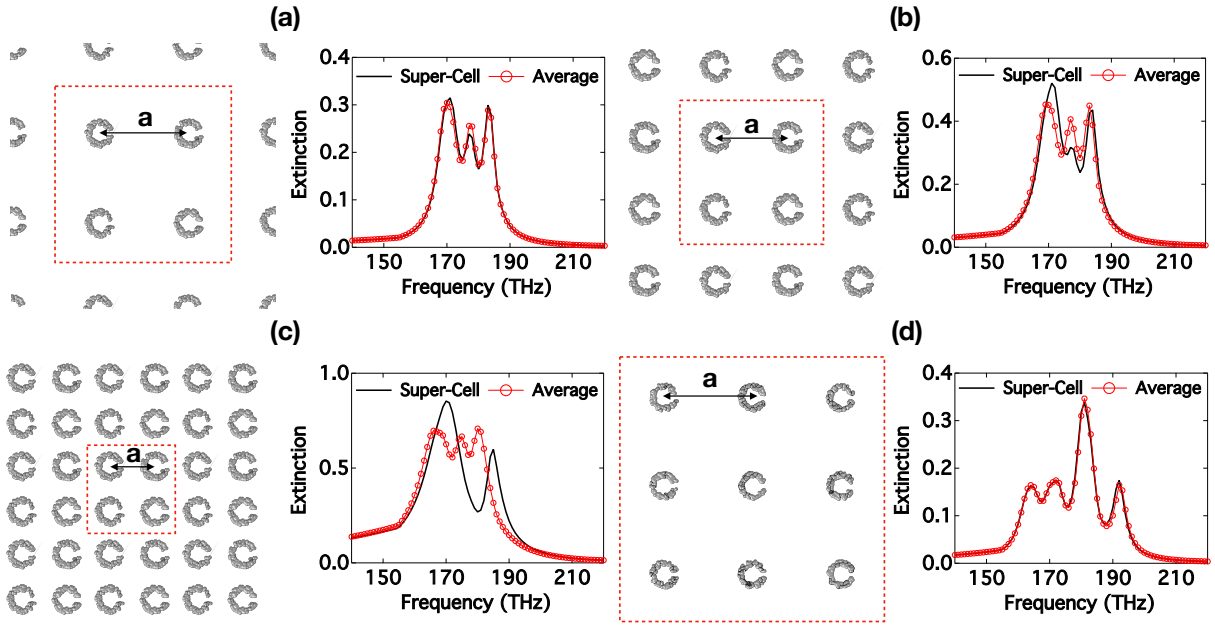

FIG. 2. Effect of inter-unit-cell interactions: Extinction spectra of super-cells in comparison to the averaged response of the composing SRRs. (a), (b) and (c) are for 2×2 super-cell SRRs with element separation a being 400, 300, and 200 nm, respectively. (d) is for a 3×3 super-cell SRR with $a = 400$ nm.

elements, but also by comparing it to the averaged response of individual structures, we are able to directly examine the effect of mutual coupling. An an example, we arbitrarily pick four different structures from the generated 100 "moderately rough"-SRR samplings, i.e., No. 64, 65, 73 and 49, forming a 2×2 supercell with the spacing between elements a. In Figs. 2(a)-(c), we show schematically the supercell array at three different spacings, i.e., a = 400, 300 and 200 nm, respectively, with the SRRs packing gradually getting denser with decreasing lattice constant a. Next to each configuration, we show the comparison of supercell response (solid black curve) and averaged response of individual SRRs (red-symbol curve) in the extinction spectra, i.e., $1 - |T|^2$, where the $|T|^2$ represents the transmitted energy for the same polarization of excitation. Unlike the supercell response, which can be directly obtained from the simulation, the average extinction spectrum is based on a two-step procedure: First, at each spacing level, we conduct the simulation to a periodic array of each individual composing SRR for S-parameters, from which we retrieve the corresponding effective σ_e; second, with the inverse of the retrieval, we translate the averaged σ_e to the averaged response in extinction. In Fig. 2(a), we can see excellent agreement between

the supercell and average response, indicating that the mutual coupling between SRRs is weak and essentially negligible at the relevant spacing level of $a = 400$ nm. When the spacing a decreases to 300 nm, we find a noticeable difference between the supercell and average response [see Fig. 2(b)], which indicates the existence of considerable interactions of neighboring building blocks in the supercell. Upon further decreasing a to 200 nm, SRRs are more densely packed together, and Fig. 2(c) shows a significant deviation between the two response curves, a clear indication of strong mutual coupling of elements at this inter-element spacing. In addition, Fig. 2(d) shows an example of 3×3 supercell, which is built by 9 randomly chosen SRRs from the 100 samplings, i.e., No. 72, 86, 38, 26, 22, 15, 33, 27 and 42, and displays a nearly-perfectly overlapped extinction spectra for the supercell and average response, further indicating that a spacing level $a = 400$ nm is sufficient for neglecting the mutual coupling of neighboring SRRs. It should also be noted that the scattering response of the metasurface fundamentally differs from that of a single scattering meta-atom, even for the case of negligible (near-field) mutual coupling between neighoring SRRs because the interference of the propagating collective far-fields of the SRRs also changes the effective strength and radiative damping for the local resonantors in the metasurface (see the Supporting Information, section V for a more detailed discussion).

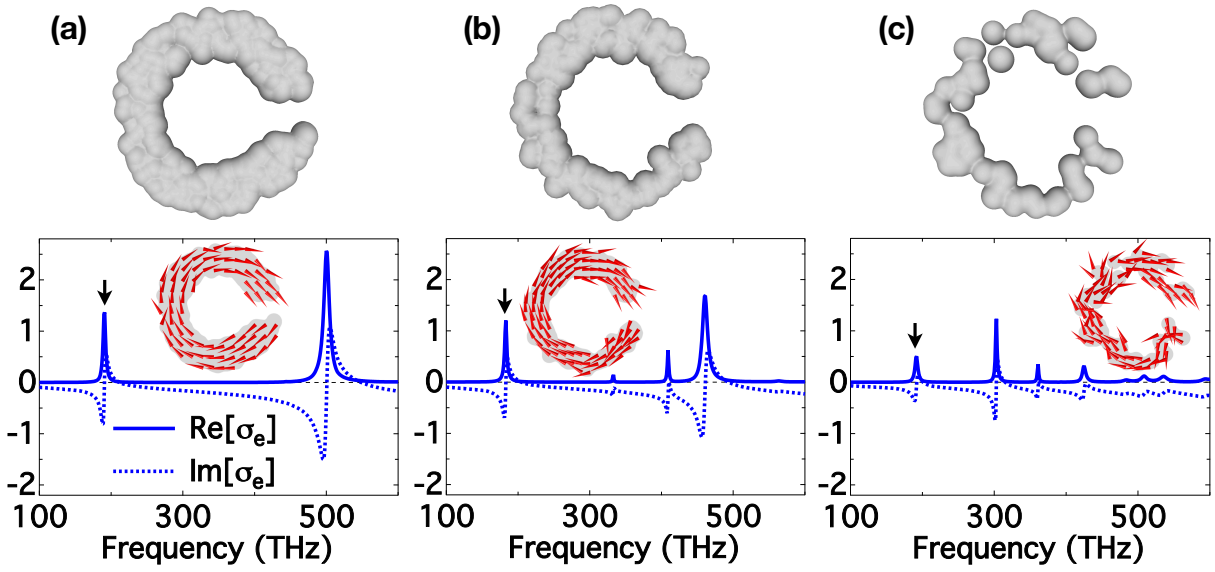

FIG. 3. Effect of disorder strength: Split-ring structures constructed with 300 (a), 120 (b) and 60 (c) random spheres and corresponding retrieved sheet electric conductivity. The insets show the current distribution of the lowest resonance mode, i.e., electrically-excited magnetic mode.

We further explore the robustness of the optical responses of the SRRs, especially the magnetic resonance, with respect to different levels of surface roughness. Although the goal for the experimental metallization process is to produce a smooth, conformal coating of the DNA template, the fundamental nature of the nucleation and growth process will ultimately result in some level of roughness. Therefore, it is essential to obtain an estimate to understand and predict at what level of disorder the fabricated meta-atoms are still expected to yield usable resonant response. To compare to the case of "moderately rough" SRRs formed by 120 spheres in the above, we construct two other sets of rough SRRs, which have either 300 or 60 spheres, with radii still randomly between 8-9 nm, positioned inside of the designed ideal SRR profile [see Fig. 1(b)]. These are denoted as "fairly smooth" (300 spheres) and "very rough" SRRs (60 spheres), respectively. For both levels of roughness, we randomly generate ensembles of 100 samples each. Sections II and III of the Supporting Information show the portraits of all the SRRs, next to which is the calculated spectrum of sheet electric conductivity σ_e for the metasurface of periodic SRRs with lattice constant 400 nm under the same polarized excitation. In Fig. 3, we show randomly chosen representatives No. 91 and 27 from the generated 300- (a) and 60-sphere (c) ensembles, respectively, together with another 120-sphere (b) sampling, i.e., No. 22, for an intuitive comparison. It is seen in Fig. 3(a), the σ_e-spectrum of the "fairly smooth" SRR example shows two clear resonance features, corresponding to the magnetic and electric dipole modes, respectively, and we show the circulating current distribution of the SRR in the inset to identify the nature of the resonance at ∼191 THz (position indicated by the black arrow). The "moderately rough" SRR example in Fig. 3(b) has very similar overall response as the one in Fig. 1, i.e., a magnetic resonance, with corresponding current distribution shown in the inset, exists at the low frequency side ∼183 THz, and several higher order modes occur above 300 THz. In contrast to these, the response of the "very rough" SRRs, indicates that this structure composed of 60 spheres is insufficient to form a continuous ring path, which leads to segmentation into multiple isolated fragments instead (see the Supporting Information, section III). Due to the complicated morphology and topology of the "very rough" SRRs, the corresponding optical response becomes very unstable, i.e., various local resonance modes may exist and even the magnetic resonance will delocalize over a broadband range. For the "very rough" SRR example in Fig. 3(c), a series of resonance features is observed within 100-600 THz of σ_e-spectrum, and even though our targeted magnetic resonance survives for

this specific example (see the current distribution in the inset at ∼192 THz), the robustness of the mode is weak in view of the responses of other samples at this level of disorder.

We have seen that all of the 100 randomly generated "fairly smooth" SRR samples show two prominent resonance features within 100-600 THz, indicating very robust optical responses of SRRs at this roughness level comparable to the response of the smooth ideal SRR. However, it should also be noted there exists some variation of the location of each mode depending on the specific morphology of each sample structure and some additional local resonance modes may appear, but they are quite weak (see the Supporting Information, section II). In order to compare the distribution of resonance features, we analyze the distribution of resonance frequencies for the magnetic and electric dipole modes. To do so, we apply the following two-mode Lorentz model to fit each retrieved σ_e spectrum: $\sigma_e = \frac{i\omega C_1}{(\omega^2-\omega_1^2)+i\omega\gamma_1} + \frac{i\omega C_2}{(\omega^2-\omega_2^2)+i\omega\gamma_2} - i\omega B$, where the first two terms are from the Lorentz response of the susceptibility χ_e for each mode ($\sigma_e = -i\omega\epsilon_0\chi_e$ with ϵ_0 free-space permittivity) and the third term is due to the background response of χ_e, summarily contributed by all other higher-order modes at higher frequencies. The circular frequencies $\omega_{1,2} = 2\pi f_{1,2}$ and collision frequencies $\gamma_{1,2}$ of the two modes, together with the coefficients $C_{1,2}$ and B are the parameters to be determined in the fitting. Following the excellent agreement between the retrieved σ_e spectra and fittings (not shown), we extract the fitted f_1 and f_2 values of all 100 samples and plot the histogram in Fig. 4(a) showing the distribution of two modes in the spectrum. The actual numeric values are provided in Table S1 in the Supporting Information, section VII. The locations of the magnetic and electric dipole modes are around 195 and 505 THz, respectively, both following normal distributions [red lines in Fig. 4(a)]. Therefore, we can see at the "fairly smooth" level, SRRs constructed with 300 random spheres possess very robust optical resonance properties.

Above we have shown that the mutual coupling between SRRs can be negligible upon the meta-atom separation, a, reaching 400 nm, which allows us to estimate the overall collective response of an SRR metasurface composed of different structures with the average response of individual composing elements. Therefore, based on the previously obtained responses of 100 random SRR samples for each level of roughness at $a = 400$ nm, we show the calculated averaged spectra of σ_e in Figs. 4(b)-(d) correspondingly. For "fairly smooth" SRRs, the average σ_e spectrum in Fig. 4(b) shows two distinct and smooth resonance features within 100-600 THz, which strongly supports the robustness of optical responses at this level of

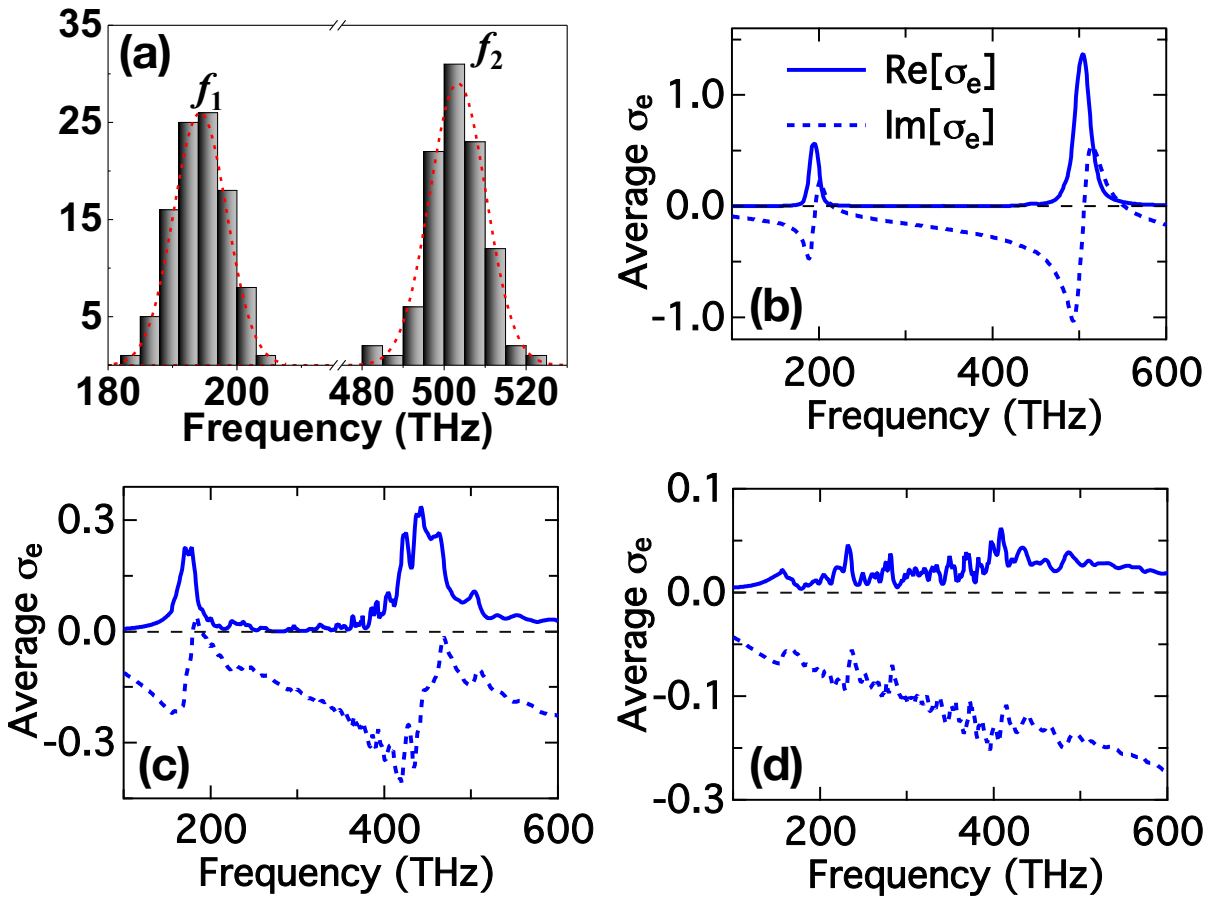

FIG. 4. Histogram of the fitted resonance frequencies for the two modes of 100 SRR samples constructed from 300 random spheres each (a). Averaged sheet electric conductivities of 100 sample SRRs formed by (b) 300, (c) 120, and (d) 60 random spheres.

profile roughness. According to the Lorentz fitting, the average magnetic and electric dipole modes occur at ∼194 and 503 THz with corresponding Q-factors of 18 and 28, respectively (see the Supporting Information, section II). The average response of σ_e for the 100 samples of "moderately rough" SRRs is presented in Fig. 4(c). This sample also shows two distinct major resonance features with well suppressed response in-between. We find the average σ_e spectrum can still be described with the Lorentz model reasonably well and the fitting gives the resonance frequencies of the two modes ∼172 and 445 THz, respectively, with both Q-factors ∼8 (see the Supporting Information, section I). Therefore, despite the fact that the "moderately rough" SRRs in general show quite complicated response spectra with multiple hybridized and local resonance modes due to structural randomness, we observe very robust magnetic and electric dipole modes, although with some broadening effect when including

the variation from a large number of SRR sampling. Finally, when the SRRs are constructed by only 60 spheres, reaching the "very rough" profile level, the average σ_e spectrum becomes very noisy throughout the frequency band under investigation, as shown in Fig. 4(d), where we cannot see any distinguishable resonance features. It is further instructive to visualize the distributiion of resonance frequencies, line width, and peak absorptions for the studied ensembles of random SRRs at all three disorder levels. This data and discussion is provided in section VI of the Supporting Information and in perfect agreement with the result presented above.

CONCLUSIONS

In conclusion, we have investigated the robustness of the optical responses for metamaterials made of meta-atoms with random morphological disorder and surface roughness, which commonly exists in metallic nano-resonators fabricated with bottom-up approach. Specifically, we develop an aggregated-random-spheres model to mimic the nucleated growth of the metallization on the DNA origami templates for realistic, experimentally observed morphological disorder and rough surface profiles. We show that while increasing structural imperfections leads to progressive Gaussian broadening of the distribution of intended resonance frequencies of the meta-atoms and to the excitation of more hybridized modes, the fundamental resonances of deeply subwavelength meta-atoms are remarkably robust against morphological disorder and surface roughness. Only extreme disorder, causing the segmentation of SRRs, results in loss of a distinct resonant response of the fundamental mode. These results are very inspiring toward achieving versatile practical metadevices with bottom-up approach and will substantially encourage further experimental studies.

ACKNOWLEDGEMENTS

Work at Ames Laboratory was supported by the US Department of Energy, Office of Basic Energy Science, Division of Materials Science and Engineering (Ames Laboratory is operated for the US Department of Energy by Iowa State University under contract No. DE-AC02-07CH11358). Work at FORTH was supported by the European Research Council under the ERC Advanced Grant No. 320081 (PHOTOMETA).

* nhshen@ameslab.gov

[1] N. Engheta, Science **317**, 1698 (2007).

[2] V. M. Shalaev, Nat. Photon. **1**, 41 (2007).

[3] B. Luk'yanchuk, N. I. Zheludev, S. A. Maier, N. J. Halas, P. Nordlander, H. Giessen, and C. T. Chong, Nat. Mater. **9**, 707 (2010).

[4] Y. Liu and X. Zhang, Chem. Soc. Rev. **40**, 2494 (2011).

[5] C. M. Soukoulis and M. Wegener, Nat. Photon. **5**, 523 (2011).

[6] N. I. Zheludev and Y. S. Kivshar, Nat. Mater. **11**, 917 (2012).

[7] S. A. Cummer, J. Christensen, and A. Alù, Nat. Rev. Mater. **1**, 16001 (2016).

[8] A. Biswas, I. S. Bayer, A. S. Biris, T. Wang, E. Dervishi, and F. Faupel, Adv. Colloid Interface Sci. **170**, 2 (2012).

[9] H.-T. Chen, W. J. Padilla, J. M. O. Zide, A. C. Gossard, A. J. Taylor, and R. D. Averitt, Nature **444**, 597 (2006).

[10] N. I. Landy, S. Sajuyigbe, J. J. Mock, D. R. Smith, and W. J. Padilla, Phys. Rev. Lett. **100**, 207402 (2008).

[11] Z. Liu, H. Lee, Y. Xiong, C. Sun, and X. Zhang, Science **315**, 1686 (2007).

[12] J. K. Gansel, M. Thiel, M. S. Rill, M. Decker, K. Bade, V. Saile, G. von Freymann, S. Linden, and M. Wegener, Science **325**, 1513 (2009).

[13] H.-T. Chen, W. J. Padilla, M. J. Cich, A. K. Azad, R. D. Averitt, and A. J. Taylor, Nat. Photon. **3**, 148 (2009).

[14] J. Valentine, J. Li, T. Zentgraf, G. Bartal, and X. Zhang, Nat. Mater. **8**, 568 (2009).

[15] N. K. Grady, J. E. Heyes, D. R. Chowdhury, Y. Zeng, M. T. Reiten, A. K. Azad, A. J. Taylor, D. A. Dalvit, and H. T. Chen, Science **340**, 1304 (2013).

[16] N. Yu, P. Genevet, M. A. Kats, F. Aieta, J.-P. Tetienne, F. Capasso, and Z. Gaburro, Science **334**, 333 (2011).

[17] A. V. Kildishev, A. Boltasseva, and V. M. Shalaev, Science **339**, 1232009 (2013).

[18] N. Yu and F. Capasso, Nat. Mater. **13**, 139 (2014).

[19] H. T. Chen, A. J. Taylor, and N. Yu, Reports Prog. Phys. **79**, 076401 (2016).

[20] D. Neshev and I. Aharonovich, Light Sci. Appl. **7**, 58 (2018).

[21] K. Wang, J. G. Titchener, S. S. Kruk, L. Xu, H. P. Chung, M. Parry, I. I. Kravchenko, Y. H. Chen, A. S. Solntsev, Y. S. Kivshar, D. N. Neshev, and A. A. Sukhorukov, Science **361**, 1104 (2018).

[22] N. Liu, H. Guo, L. Fu, S. Kaiser, H. Schweizer, and H. Giessen, Nat. Mater. **7**, 31 (2008).

[23] W. Wu, Z. Yu, S. Y. Wang, R. S. Williams, Y. Liu, C. Sun, X. Zhang, E. Kim, Y. R. Shen, and N. X. Fang, Appl. Phys. Lett. **90**, 063107 (2007).

[24] I. Bergmair, B. Dastmalchi, M. Bergmair, A. Saeed, W. Hilber, G. Hesser, C. Helgert, E. Pshenay-Severin, T. Pertsch, E. B. Kley, U. Hübner, N. H. Shen, R. Penciu, M. Kafesaki, C. M. Soukoulis, K. Hingerl, M. Muehlberger, and R. Schoeftner, Nanotechnology **22**, 325301 (2011).

[25] M. S. Rill, C. Plet, M. Thiel, I. Staude, G. Von Freymann, S. Linden, and M. Wegener, Nat. Mater. **7**, 543 (2008).

[26] S. A. DiBenedetto, A. Facchetti, M. A. Ratner, and T. J. Marks, Adv. Mater. **21**, 1407 (2009).

[27] P. W. Rothemund, Nature **440**, 297 (2006).

[28] A. V. Pinheiro, D. Han, W. M. Shih, and H. Yan, Nat. Nanotechnol. **6**, 763 (2011).

[29] S. J. Tan, M. J. Campolongo, D. Luo, and W. Cheng, Nat. Nanotechnol. **6**, 268 (2011).

[30] F. Hong, F. Zhang, Y. Liu, and H. Yan, Chem. Rev. **117**, 12584 (2017).

[31] N. Liu and T. Liedl, Chem. Rev. **118**, 3032 (2018).

[32] A. Kuzyk, R. Jungmann, G. P. Acuna, and N. Liu, ACS Photon. **5**, 1151 (2018).

[33] A. Kuzyk, R. Schreiber, Z. Fan, G. Pardatscher, E. M. Roller, A. Högele, F. C. Simmel, A. O. Govorov, and T. Liedl, Nature **483**, 311 (2012).

[34] R. Schreiber, S. Kempter, S. Holler, V. Schüller, D. Schiffels, S. S. Simmel, P. C. Nickels, and T. Liedl, Small **7**, 1795 (2011).

[35] J. Liu, Y. Geng, E. Pound, S. Gyawali, J. R. Ashton, J. Hickey, A. T. Woolley, and J. N. Harb, ACS Nano **5**, 2240 (2011).

[36] Y. Geng, J. Liu, E. Pound, S. Gyawali, J. N. Harb, and A. T. Woolley, J. Mater. Chem. **21**, 12126 (2011).

[37] Z. Jin, W. Sun, Y. Ke, C. J. Shih, G. L. Paulus, Q. Hua Wang, B. Mu, P. Yin, and M. S. Strano, Nat. Commun. **4**, 1663 (2013).

[38] W. Sun, E. Boulais, Y. Hakobyan, W. L. Wang, A. Guan, M. Bathe, and P. Yin, Science **346**, 1258361 (2014).

[39] M. M. Hossen, L. Bendickson, P. E. Palo, Z. Yao, M. Nilsen-Hamilton, and A. C. Hillier, Nanotechnology **29**, 355603 (2018).

[40] B. Shen, V. Linko, K. Tapio, S. Pikker, T. Lemma, A. Gopinath, K. V. Gothelf, M. A. Kostiainen, and J. J. Toppari, Sci. Adv. **4**, eaap8978 (2018).

[41] K. Aydin, K. Guven, N. Katsarakis, C. M. Soukoulis, and E. Ozbay, Opt. Express **12**, 5896 (2004).

[42] A. A. Zharov, I. V. Shadrivov, and Y. S. Kivshar, Journal of Applied Physics **97**, 113906 (2005), https://doi.org/10.1063/1.1923591.

[43] M. V. Gorkunov, S. A. Gredeskul, I. V. Shadrivov, and Y. S. Kivshar, Phys. Rev. E **73**, 056605 (2006).

[44] J. Gollub, T. Hand, S. Sajuyigbe, S. Mendonca, S. Cummer, and D. R. Smith, Applied Physics Letters **91**, 162907 (2007), https://doi.org/10.1063/1.2801391.

[45] N. Papasimakis, V. A. Fedotov, Y. H. Fu, D. P. Tsai, and N. I. Zheludev, Phys. Rev. B **80**, 041102 (2009).

[46] C. Helgert, C. Rockstuhl, C. Etrich, C. Menzel, E.-B. Kley, A. Tünnermann, F. Lederer, and T. Pertsch, Phys. Rev. B **79**, 233107 (2009).

[47] J. Zhou, T. Koschny, M. Kafesaki, E. N. Economou, J. B. Pendry, and C. M. Soukoulis, Phys. Rev. Lett. **95**, 223902 (2005).

[48] P. B. Johnson and R. W. Christy, Phys. Rev. B **6**, 4370 (1972).

[49] P. Tassin, T. Koschny, and C. M. Soukoulis, Phys. B Condens. Matter **407**, 4062 (2012).